2.2. Peptides

Peptides 35 to 55 of myelin-oligodendrocyte glycoprotein (MOG_{35-55}; single-letter amino acid code: MEVGWYRSPFSRVVHLYRNGK) were purchased from Tore Research Institute (Tore Research, Tokyo, Japan). The peptides were >90% pure, as determined by high performance liquid chromatography (HPLC).

2.3. Induction and evaluation of EAE

Mice were injected subcutaneously in the flan, bilaterally, with 0.2 mL of inoculums containing 100 mg of MOG_{35-55} and 0.5 mg of mycobacterium tuberculosis H37RA (Difco Laboratories, Detroit, MI) in incomplete Freund's adjuvant. Mice were given 300 ng of pertussis toxin (Sigma-Aldrich, St. Louis, MO) intraperitoneally on day 0 and day 2 postimmunization. Immunized mice were examined daily and scored as follows: 0, no clinical signs; 1, limp tail; 2, partial hind leg paralysis; 3, total hind leg or partial hind and front leg paralysis; 4, total hind leg and partial front leg paralysis; and 5, moribund or dead. Mice were examined daily for signs of EAE in a blind fashion (Miyamoto et al., 2001).

2.4. T cell proliferation assay

For the proliferation assay, mice were immunized with peptides/CFA as described above, but they were not treated with pertussis toxin. A single-cell suspension was prepared from the draining lymph nodes (LNs) and spleen on day 11 after immunization. Cells were cultured in RPMI GlutaMAX (Gibco, Grand Island, NY) supplemented with 5% heat-inactivated fetal bovine serum (FBS), and seeded onto 96-well flat-bottomed plates (5×10^5 cells/well). The cells were restimulated with peptide for 48 h at 37 °C under a humidified air condition with 5% CO_2. To measure cellular proliferation, [^{3}H]-thymidine was added (1 μCi/well) and uptake of the radioisotope during the final 18 h of culture was counted with a beta-1205 counter (Pharmacia, Uppsala, Sweden). To evaluate proliferative responses of LN and spleen cells to the peptide, we determined the Δcpm values for cells in each well by subtracting the background cpm and used the mean of these values to represent each mouse.

2.5. Cytokine capture beads assay

In parallel, the LN cells from immunized mice were cultured with peptide concentrations of 0, 1, 10, and 100 μg/mL. Supernatants from the cultures were harvested 48 h post activation and tested for the presence of various cytokines. The concentrations of interleukin (IL)-2, IL-4, IL-6, IL-10, IL-17a, interferon (IFN)-γ, and tumor necrosis factor (TNF) were measured by using a capture beads assay (BD Bioscience). The assay was performed according to the manufacturer's guidelines.

2.6. Pathological analysis

On day 35 after immunization, mice were sacrificed. Brains and spinal cords were harvested and fixed in 10% neutral buffered formalin. Paraffin sections were stained with hematoxylin and eosin (HE) to assess inflammation, and Klüver–Barrera stain to assess demyelination.

2.7. Analysis of infiltrating cells isolated from the central nervous system

Wild type (WT) and DKO mice were anesthetized with diethyl ether on day 14 after induction of EAE. After perfusion with PBS, brains and spinal cords were harvested and homogenized. After washing with PBS, mononuclear cells were isolated using Percoll gradient (GE Healthcare, Uppsala, Sweden) and counted (Miyamoto et al., 2006). As a control, the central nervous system (CNS)-infiltrated cells in naïve mice were also analyzed following the same method.

2.8. Flow cytometry

Single-cell suspensions were obtained from the spleen and CNS as described above. Briefly, 2×10^6 cells were placed in each tube with 100 μL of 3% FBS in PBS, and flow cytometric analysis was performed. Three-color analysis was performed with a combination of fluorescein isothiocyanate (FITC)-conjugated anti-mouse CD4, allophycocyanin (APC)-conjugated anti-mouse CD3, and phycoerythrin (PE)-conjugated anti-mouse CCR6, CCR4, or purified hamster IgG (BD PharMingen, San Diego, CA). After Fc-block, samples were stained on ice with predetermined optimal concentrations of antibodies for 30 min, and analyzed on a flow cytometer (BD FACS Calibur). The assay for detecting regulatory T cell was performed using a mouse regulatory T cell staining kit according to the manufacture's guidelines (eBioscience).

3. Results

3.1. $CCR6^{-/-}CCR4^{-/-}$ DKO mice generation

$CCR6^{-/-}CCR4^{-/-}$ mice were generated by mating $CCR6^{+/-}$ and $CCR4^{+/-}$ mice. Intercrosses between the $CCR6^{+/-}CCR4^{+/-}$ mice gave rise to 34 DKO homozygous, 96 CCR6 homozygous, 90 CCR4 homozygous, and 295 mice of other genotypes, nearly proportional to the Mendelian inheritance pattern of 1:3:3:9. The genotype of DKO mice was confirmed by employing a PCR method using tail genomic DNA to amplify a 621-bp product from the WT allele and a 429-bp product from the CCR6 null allele in $CCR6^{-/-}$ mice, and a 1089-bp product from the WT allele and a 197-bp product from the CCR4 null allele in $CCR4^{-/-}$ mice (Fig. 1A). DKO mice were healthy and no particular changes were found in their gross appearance (Fig. 1B).

3.2. Disease severity was suppressed in DKO mice

To examine the role of CCR6 and CCR4 in EAE, C57BL/6 WT control mice (WT, n=26), $CCR6^{-/-}$ (6KO, n=17), $CCR4^{-/-}$ (4KO, n=22), and DKO (n=18) were immunized to establish EAE. There were no significant differences in disease incidence (DKO, 77.8%; 6KO, 82.4%; 4KO, 77.3%; and WT, 84.5%). However, DKO exhibited delayed disease onset and less severe disease activity (Fig. 2A). Twenty days after immunization was required to develop neurological symptoms in 50% of DKO mice, whereas 50% of WT mice required 16 days

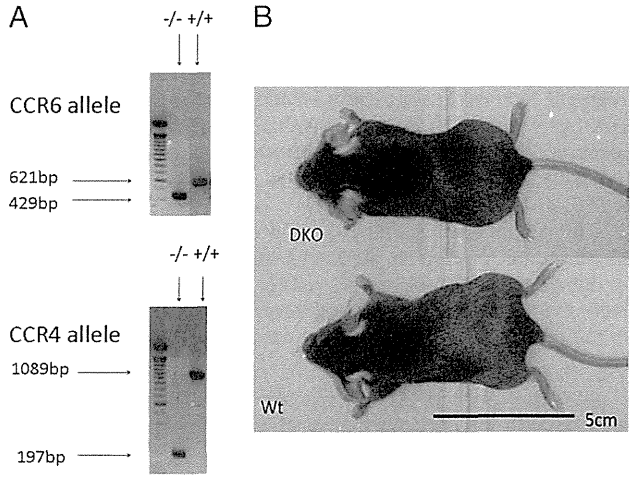

Fig. 1. Generation of double knockout (DKO) mice. A, Genotyping by polymerase chain reaction using genomic DNA. The upper picture shows a 621-bp product from the wild type (WT) allele and a 429-bp product from the CCR6 null allele, and the lower picture shows a 1089-bp product from the WT allele and a 197-bp product from the CCR4 null allele. B, Gross appearance of 8-week-old female DKO and WT mice. No particular change was found.

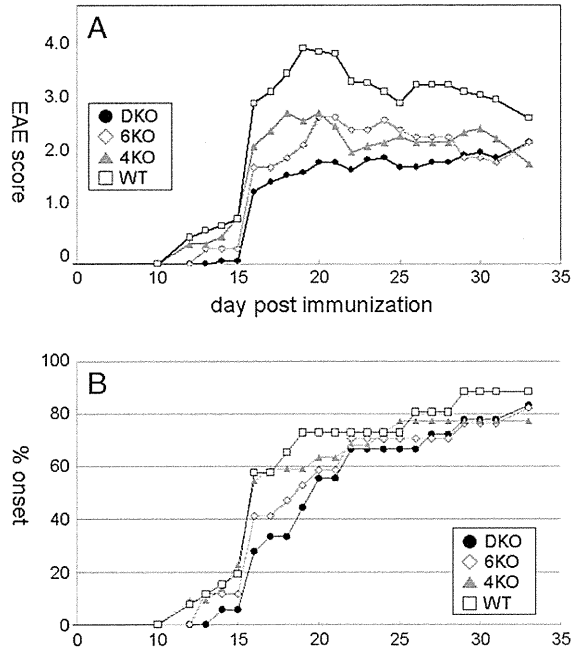

Fig. 2. EAE was induced in double knockout (DKO, n = 18), CCR6 knockout (6KO, n = 17), CCR4 knockout (4KO, n = 22), and wild type (WT, n = 26) mice by immunization with MOG_{35-55} in complete Freund's adjuvant and monitored daily for symptoms of EAE. A, DKO mice developed less severe EAE. Summaries of disease features are shown in Table 1. B, Delayed disease onset in DKO mice is shown. In order to note neurological symptoms in 50% of DKO, 6KO, 4KO, and WT mice, 20, 18, 16, and 16 days were required, respectively.

(Fig. 2B). With regard to the severity of EAE, DKO showed least severe EAE among all groups and a significantly lower score on day 19 (DKO, 1.29 ± 0.31; 6KO, 1.38 ± 0.36; 4KO, 1.66 ± 0.34; WT, 2.95 ± 0.37, [mean ± SEM]). The cumulative EAE score was as follows: DKO, 23.0 ± 3.3; 6KO, 29.9 ± 5.1; 4KO, 34.1 ± 4.0; and WT, 43.5 ± 4.5. The maximum clinical score was as follows: DKO, 2.82 ± 0.25; 6KO, 3.10 ± 0.28; 4KO, 3.18 ± 0.23; and WT, 3.52 ± 0.18. Pathological changes in spinal cord sections were also evaluated. DKO mice exhibited less mononuclear infiltration than WT mice. Summaries of disease features are shown in Table 1 and Fig. 2.

3.3. Lack of CCR6 and CCR4 reduces uptake of [^{3}H]-thymidine in MOG-specific T cells

The proliferative response of draining LNs and spleens of in vitro DKO, or WT immunized with MOG_{35-55} was evaluated. On day 11 after immunization, bilateral inguinal LNs and spleens were harvested and the cells of prepared single-cell suspensions were counted. No particular change was found in spleens collected from DKO mice compared with naïve mice, whereas WT mice developed splenomegaly. The cell count from spleens of DKO mice was lower than that of WT mice (DKO, n = 6, 83.0 ± 8.5 × 10^6; WT, n = 7, 101.6 ± 9.9 × 10^6, Fig. 3A). Uptake of [^{3}H]-thymidine was also significantly downregulated in spleen cells of DKO mice (9100 ± 868 versus 15923 ± 3799, $P<0.05$, Fig. 3B). In cells from LNs, there was no significant difference.

Table 1
Summary of clinical experimental autoimmune encephalomyelitis (EAE).

	Incidence	Day of onset	Max score	Cumulative score
DKO (n = 18)	77.8% (14/18)	20.4 ± 1.36	2.82 ± 0.25*	23.0 ± 3.3**
6KO (n = 17)	82.4% (14/17)	19.4 ± 1.43	3.10 ± 0.28	29.9 ± 5.1*
4KO (n = 22)	77.3% (17/22)	17.1 ± 0.92	3.18 ± 0.23	34.1 ± 4.0
WT (n = 26)	84.5% (22/26)	18.2 ± 1.01	3.52 ± 0.18	43.5 ± 4.5

Mean ± standard error.
DKO, double knockout; 6KO, chemokine receptor 6 knockout; 4KO, chemokine receptor 4 knockout; WT, wild type.
**p<0.001, *p<0.05 versus WT by Mann–Whitney *U* test.

3.4. IL-6 and IL-17 production was downregulated in DKO mice

The cytokine concentrations in the culture supernatants were estimated by using a cytometric bead assay (CBA). IL-6 and IL-17a production was significantly lower in DKO mice than in WT mice (IL-6, 16.1 ± 4.9 versus 49.4 ± 9.2; IL-17a, 17.4 ± 2.5 versus 38.3 ± 7.4; DKO, n = 8; WT, n = 7; $P<0.01$). IFN-γ and TNF levels were also slightly lower, although not significant (IFN-γ, 295 ± 131 versus 384 ± 94; TNF, 72.9 ± 17.5 versus 100.4 ± 14.2; DKO, n = 8; WT, n = 7). IL-2, IL-4, and IL-10 were not detected. This finding might suggest that Th17 activity, rather the Th1 activity, was suppressed in DKO mice. A summary of the data is shown in Fig. 4.

3.5. Cellular infiltration into the CNS was repressed in DKO mice

We examined the isolated cells from the immunized murine CNS to analyze the role of CCRs on migration of inflammatory cells into the CNS. The number of mononuclear cells in the CNS isolated from DKO mice was less than that from WT mice (Fig. 5; DKO, n = 6, 12.5 ± 3.1 × 10^5; WT, n = 6, 17.7 ± 1.4 × 10^5; naïve, 10.2 ± 2.2 × 10^5, n = 6). In parallel, lymphocytes isolated from the CNS and spleens were analyzed by flow cytometry. Compared with peripheral T cells, CCR6 expression of infiltrated T cells in WT was increased, whereas no CCR6 expression was detected in both CNS and peripheral T cells of DKO mice (Fig. 6). Next, we evaluated the number of $CD4^+CD25^+Foxp3^+$ regulatory T cells in spleens; however, there was no significant difference between the groups (data not shown).

4. Discussion

Chemokines and CCRs play important roles in mediating various autoimmune diseases, including multiple sclerosis (MS). Many studies were conducted to identify an association between EAE and CCRs, expecting they become therapeutic targets in MS. Here, we demonstrated that DKO, $CCR6^{-/-}$, and $CCR4^{-/-}$ mice developed less severe EAE. This finding suggests that CCR6 and CCR4 play an important role in deteriorating the course of EAE, especially in activating MOG-specific T cells in the induction phase. The recall response showed an inhibited T cell proliferation response and decreased Th17-associated expression of cytokines in DKO mice. The number of CNS-infiltrated cells was significantly lower in DKO mice than in WT mice. In WT mice, the CCR6 expression was increased in CNS-infiltrated T cells compared with that of splenic T cells. These results might reflect either repressed recall response or relevance of CCR6 and CCR4 to blood–brain barrier migration, which would be confirmed by adoptive transfer EAE.

Our results and the report of Forde et al. showed that CCR4 knockout reduced the severity of EAE, although no obvious CCR4 expression was observed in our study. CCR4 has been conventionally considered as a marker of Th2 activation (Koelink et al., 2011). Indeed, administration of an anti-CCR4 antibody to human healthy subjects reduced Th2-mediated cytokine production; however, it had no effect on the production of Th1-mediated cytokines (Yamane-Ohnuki and Satoh, 2009). On the other hand, Shimizu et al. reported that the numbers of $CD4^+CCR4^+$ cells and $CD8^+CCR4^+$ cells in peripheral blood of MS patients were higher in the relapsing phase than in the remission phase or in healthy controls (Shimizu et al., 2011). Recent studies showed that Th17 cells co-express CCR4 and CCR6 and that the proportions of $CCR4^+CCR6^+CD4^+$ correlate with the disease activity of MS (Mehling et al., 2010). These findings might indicate that CCR4 was necessary in activating pathogenic Th1/Th17 cells, and inhibition of Th2 cells did not necessarily mean Th1 stimulation. Recently

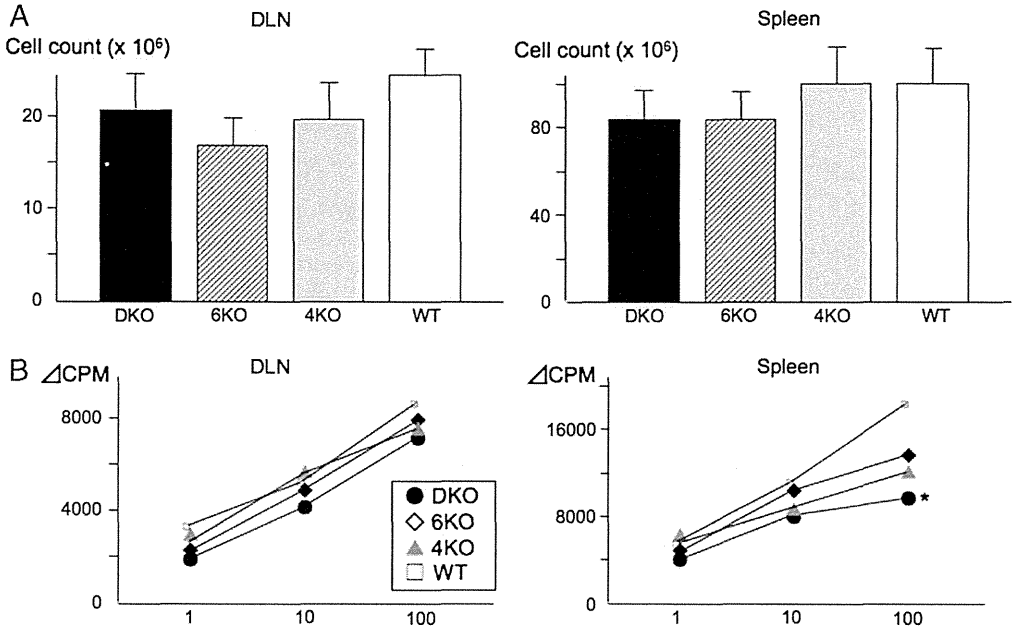

Fig. 3. Comparison of MOG_{35-55} T cell responses in DKO and WT mice. A, Cell count of lymphocytes isolated from draining lymph nodes (LN) and spleens. The cell count of cells isolated from spleens of DKO mice was lower than that of WT mice (DKO, n=6, 83.0±8.5×10⁶; WT, n=7, 101.6±9.9×10⁶). The cell count of cells harvested from LNs was also slightly decreased in DKO mice (DKO, 21.0±3.9×10⁶; WT, 24.4±3.5×10⁶). B, The proliferative response was determined by the uptake of [³H] thymidine. The value of Δcpm was significantly decreased in DKO splenic cells (9100±868, n=6 versus 15923±3799, n=7; P<0.05 by Mann–Whitney *U* test). *p<0.05 versus WT by Mann–Whitney *U* test.

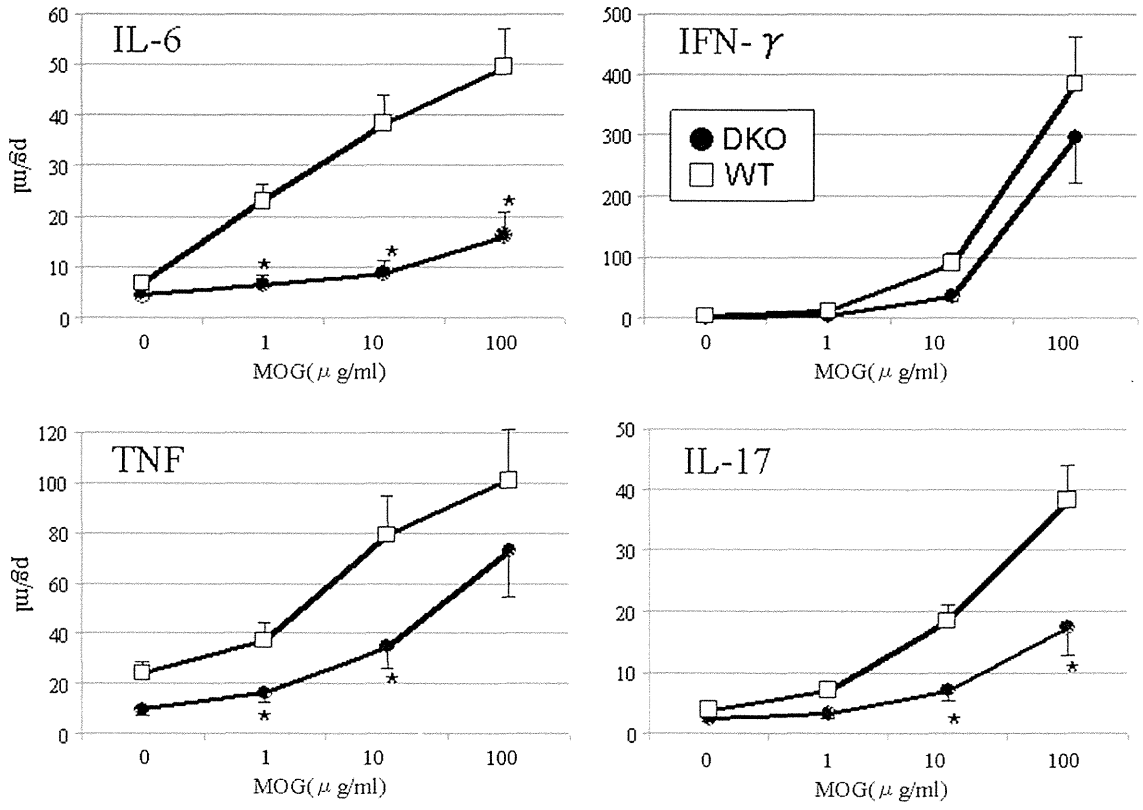

Fig. 4. Cytokine concentrations of culture supernatants were measured by using a cytometric bead assay (CBA). The production of IL-6 and IL-17a was significantly suppressed in double knock out *DKO mice (IL-6, 16.1±4.9 versus 49.4±9.2; IL-17a, 17.4±2.5 versus 38.3±7.4; DKO, n=8; WT, n=7; P<0.01 by Mann–Whitney *U* test). The production of interferon (IFN)-γ and tumor necrosis factor (TNF) was also decreased, although not significantly (IFN-γ, 295±131 versus 384±94; TNF, 72.9±17.5 versus 100.4±14.2; DKO, n=8; WT, n=7). *p<0.01 versus WT by Mann–Whitney *U* test.

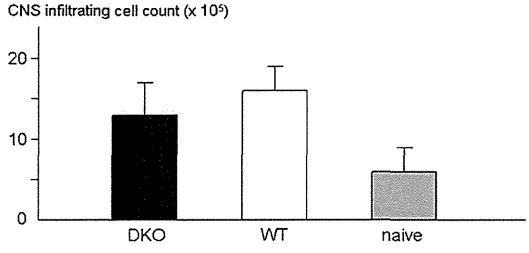

Fig. 5. Infiltrated cell count in central nervous system. Cell count of mononuclear cells isolated from the CNS of immunized mice and naïve mice. Mononuclear cell count of the CNS isolated from double knockout (DKO) mice was less than that of WT mice (DKO, $n=6$, $12.5\pm3.1\times10^5$; WT, $n=6$, $17.7\pm1.4\times10^5$; naïve, $10.2\pm2.2\times10^5$, $n=6$).

anti-CCR4 antibody has been applied in clinical trial of adult T cell leukemia. This antibody may become a novel therapeutic drug for MS.

The results of previous reports of EAE in CCR6 single knockout mice are conflicting. This discrepancy might be explained by the complexity of immune mechanisms, i.e., a single cytokine or chemokine has contrary functions in vitro, and many different immunological pathways have a similar outcome. Because disruption of IFN-γ signaling deteriorates EAE (Ferber et al., 1996), blockage of a single pathogenic pathway in the immune response might accelerate another pathway.

Our results, which focus mainly on analyzing pathogenic T cells in the priming phase, suggest that CCR6 and CCR4 are not essential for generating EAE; however, they play important roles in the more severe progression of EAE. Karpus and Kennedy showed that disease development of adoptive-transfer EAE correlated with CCL3, a ligand for CCR4 and that anti-CCL3 antibodies suppress the disease severity of EAE (Karpus and Kennedy, 1997). Buschmann et al. demonstrated that CCL3 expression correlated with demyelination and microglia/astrocyte activation in cuprizone-induced demyelination model (Buschmann et al., 2012). CCL20, a ligand for CCR6, is also known to be secreted by astrocyte and contribute to the disease course during EAE (Ambrosini et al., 2003). Our result might reflect abolishment of CCL3-CCR4 or CCL20-CCR6 signaling and subsequent inhibition of microglia/astrocyte activation.

Although further researches are required to assess the role of CCR in the effecter phase of EAE and the involvement of other immune-mediating cell populations expressing CCRs or their ligands, their regulation might be a therapeutic target of human inflammatory demyelinating diseases.

Acknowledgment

This work was supported in part by a research grant from the Ministry of Health, Labour and Welfare of Japan.

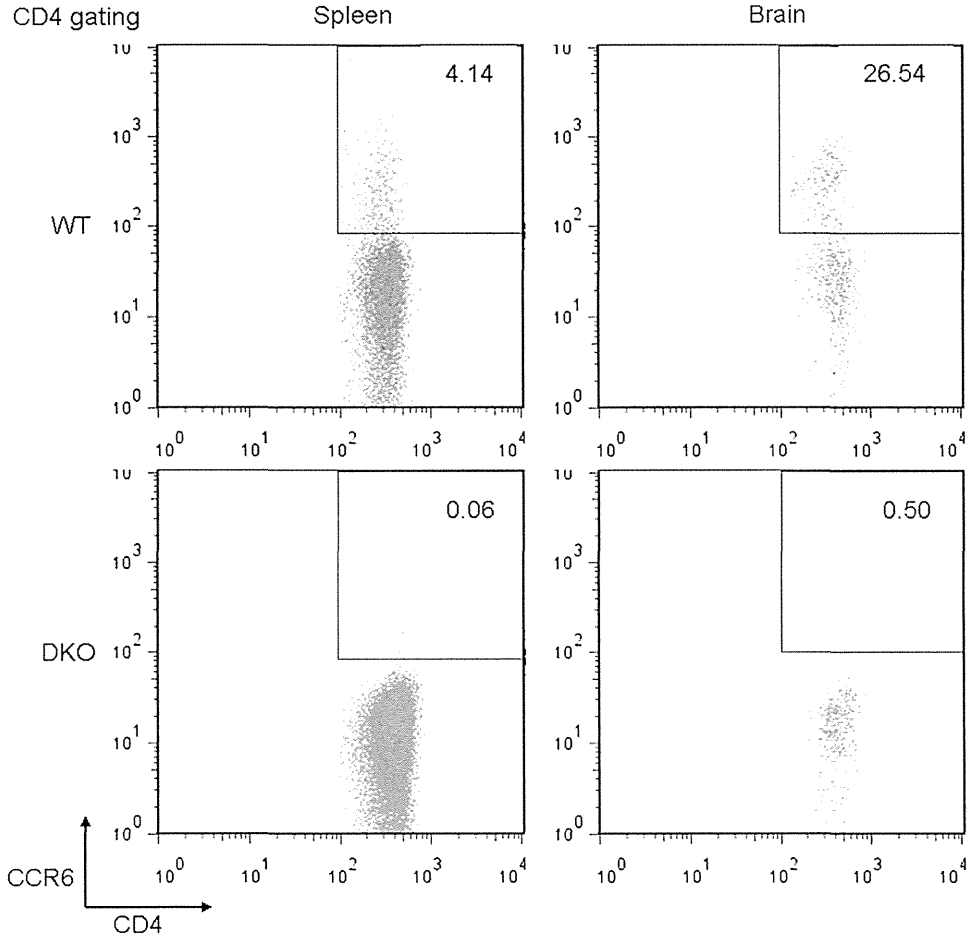

Fig. 6. Analysis of central nervous system (CNS)-infiltrated cells. In parallel, lymphocytes isolated from CNS and spleen were analyzed by flow cytometry. Compared with peripheral T cells (4.14%), CCR6 expression of infiltrated T cells in WT was increased (26.54%), whereas no CCR6 expression was detected in both peripheral (0.06%) and CNS (0.50%) T cells of DKO mice.

References

Ambrosini, E., Columba-Cabezas, S., Serafini, B., Muscella, A., Aloisi, F., 2003. Astrocytes are the major intracerebral source of macrophage inflammatory protein-3α/CCL20 in relapsing experimental autoimmune encephalomyelitis and in vitro. Glia 41, 290–300.

Aranami, T., Yamamura, T., 2008. Th17 cells and autoimmune encephalomyelitis (EAE/MS). Allergol. Int. 57, 115–120.

Buschmann, J.P., Berger, K., Awad, T., Clarner, T., Beyer, C., Kipp, M., 2012. Inflammatory response and chemokine expression in the white matter corpus callosum and gray matter cortex region during cuprizone-induced demyelination. J. Mol. Neurosci. 48, 66–76.

Domingues, H.S., Mues, M., Lassmann, H., Wekerle, H., Krishnamoorthy, G., 2010. Functional and pathogenic differences of Th1 and Th17 cells in experimental autoimmune encephalomyelitis. PLoS One 5, e15531.

Elhofy, A., DePaolo, R.W., Lira, S.A., Lukacs, N.W., Karpus, W.J., 2009. Mice deficient for CCR6 fail to control chronic experimental autoimmune encephalomyelitis. J. Neuroimmunol. 213, 91–99.

Ferber, I.A., Brocke, S., Taylor-Edwards, C., Ridgway, W., Dinesco, C., Steinman, R., et al., 1996. Mice with a disrupted IFN-γ gene are susceptible to the induction of experimental autoimmune encephalomyelitis (EAE). J. Immunol. 156, 5–7.

Forde, E.A., Dogan, R.E., Karpus, W.J., 2011. CCR4 contributes to the pathogenesis of experimental autoimmune encephalomyelitis by regulating inflammatory macrophage function. J. Neuroimmunol. http://dx.doi.org/10.1016/j.jneuroim.2011.04.008.

Ishida, T., Ueda, R., 2006. CCR4 as a novel molecular target for immunotherapy of cancer. Cancer Sci. 97, 1139–1146.

Karpus, W.J., Kennedy, K.J., 1997. MIP-1α and MCP differentially regulate acute and relapsing autoimmune encephalomyelitis as well as Th1/Th2 lymphocyte differentiation. J. Leukoc. Biol. 62, 681–687.

Koelink, P.J., Overbeek, S.A., Braber, S., Folkerts, G., de Kruijf, Petra, Smit, M.J., et al., 2011. Targeting chemokine receptors in chronic inflammatory diseases: an extensive review. Pharmacol. Ther. http://dx.doi.org/10.1016/j.pharmthera.2011.06.008.

Liston, A., Kohler, R.E., Townley, S., Haylock-Jacobs, S., Comerford, I., Caon, A.C., et al., 2009. Inhibition of CCR6 function reduces the severity of experimental autoimmune encephalomyelitis via effects on the priming phase of the immune response. J. Immunol. 182, 3121–3130.

Mehling, M., Lindberg, R., Raulf, F., Kuhle, J., Hess, C., Kappos, L., et al., 2010. Th17 central memory T cells are reduced by FTY720 in patients with multiple sclerosis. Neurology 75, 403–410.

Miyamoto, K., Miyake, S., Yamamura, T., 2001. A synthetic glycolipid prevents autoimmune encephalomyelitis by inducing TH2 bias of natural killer T cells. Nature 413, 531–534.

Miyamoto, K., Miyake, S., Mizuno, M., Oka, N., Kusunoki, S., Yamamura, T., 2006. Selective COX-2 inhibitor celecoxib prevents experimental autoimmune encephalomyelitisthrough COX-2-independent pathway. Brain 129, 1984–1992.

Nakatani, T., Kaburagi, Y., Shimada, Y., Inaoki, M., Takehara, K., Mukaida, N., et al., 2001. CCR4+ memory CD4+ T lymphocytes are increased in peripheral blood and lesional skin from patients with atopic dermatitis. J. Allergy Clin. Immunol. 107, 353–358.

Reboldi, A., Coisne, C., Baumjohann, D., Benvenuto, F., Bottinelli, D., Lira, S., et al., 2009. C-C chemokine receptor 6-regulated entry of TH-17 cells into the CNS through the choroid plexus is required for the initiation of EAE. Nat. Immunol. 10, 514–523.

Shimizu, Y., Ota, K., Kubo, S., Kabasawa, C., Kobayashi, M., Ohashi, T., et al., 2011. Association of Th1/Th2-related chemokine receptors in peripheral T cells with disease activity in patients with multiple sclerosis and neuromyelitis optica. Eur. Neurol. 66, 91–97.

Villares, R., Cadenas, V., Lozano, M., Almonacid, L., Zaballos, A., Martı´nez-A, C., et al., 2009. CCR6 regulates EAE pathogenesis by controlling regulatory CD4+ T-cell recruitment to target tissues. Eur. J. Immunol. 39, 1671–1681.

Yamane-Ohnuki N., Satoh M., 2009. Production of therapeutic antibodies with controlled fucosylation. MAbs 1, 230–236.

Vol.3, No.2, 41-46 (2013)
doi:10.4236/oji.2013.32007

Autoantibodies against myelin antigens in patients with neuromyelitis optica

Kota Moriguchi[1], Katsuichi Miyamoto[2*], Juri Ichihashi[2], Susumu Kusunoki[2]

[1]Department of Internal Medicine 3, National Defense Medical College, Tokorozawa, Japan
[2]Department of Neurology, Kinki University School of Medicine, Osaka, Japan;
*Corresponding Author: miyamoto@med.kindai.ac.jp

Received 15 March 2013; revised 14 April 2013; accepted 28 April 2013

Copyright © 2013 Kota Moriguchi *et al.* This is an open access article distributed under the Creative Commons Attribution License, which permits unrestricted use, distribution, and reproduction in any medium, provided the original work is properly cited.

ABSTRACT

In this study, we investigated the clinical relevance of anti-myelin antibodies in patients with neuromyelitis optica (NMO); titers of antibodies against myelin oligodendrocyte glycoproteins, proteolipid proteins and myelin basic proteins were measured in the sera of patients with NMO and compared to healthy controls, as well as to patients with other diseases. The frequency of presence of anti-myelin antibodies in patients with NMO was significantly higher than that in healthy and diseased controls. The expanded disability status scale scores correlated with the titers of the anti-myelin antibodies. Patients with anti-myelin antibody exhibited other autoantibodies significantly more frequently than patients without the antibody. Anti-myelin antibodies may be useful markers for predicting severe clinical courses in patients with NMO.

Keywords: Neuromyelitis Optica; Anti-Myelin Antibody; Myelin Oligodendrocyte Glycoprotein; Proteolipid Protein; Myelin Basic Protein

1. INTRODUCTION

Neuromyelitis optica (NMO) is an idiopathic and severe demyelinating, inflammatory disease that attacks the optic nerve and spinal cord. While this rare disorder resembles multiple sclerosis (MS) in several ways, recent studies have demonstrated that NMO can be clearly distinguished through its clinical course, prognosis, pathological features, and etiology. Patients with NMO often have a poor prognosis and relapsing clinical course. More than half of them develop severe visual loss or an inability to ambulate without assistance within a few years of disease onset [1]. The pathological features of NMO are characterized by immunoglobulin deposition, complement activation, vascular hyalinization and granulocyte infiltration of active lesions [2]. Based on the discovery of an autoantibody in patients with NMO, which is directed against the water channel aquaporin-4 (AQP4), NMO is now considered as an antibody-mediated autoimmune disease [3].

Proposed targets of the immune response in inflammatory demyelinating diseases of the central nervous system include myelin antigens such as myelin oligodendrocyte glycoprotein (MOG), proteolipid protein (PLP), and myelin basic protein (MBP) [4]. It has been demonstrated that antibodies against MOG can cause demyelination *in vitro* [5] and in animal models [6]. While many studies have been performed to investigate anti-myelin antibodies in patients with MS, the pathogenic or predictive role of these antibodies remains uncertain [7,8]. Few investigations have been conducted in order to evaluate the clinical relevance of anti-myelin antibodies in NMO [9]. Herein, we report on a retrospective case-control study of 17 NMO patients with anti-AQP4 antibodies in order to evaluate the clinical relevance of anti-myelin antibodies in these patients.

2. METHODS

2.1. Patients and Controls

Serum samples from 17 patients with NMO spectrum disorders, including NMO and at-risk syndromes that fulfilled the criteria proposed by Wingerchuk [10], were investigated. The serum samples were kept frozen at −80˚C until time of use. All patients with NMO had high titers of the anti-AQP4 antibody. We also investigated samples from 30 healthy controls, as well as 63 controls with the following diseases: MS (n = 21), Guillain-Barré syndrome (n = 16), chronic inflammatory demyelinating polyradiculopathy (n = 4), Miller Fisher syndrome (n = 2), cerebral infarction (n = 6) and other neurodegenera

Copyright © 2013 SciRes.

tive diseases (n = 14). Informed consent was obtained, and the study was approved by the internal review board of Kinki University Faculty of Medicine.

2.2. ELISA for Antibodies against Myelin Antigens

The presence of serum antibodies against myelin antigens was investigated with enzyme-linked immunosorbent assays (ELISA), as previously described [7]. Microtiter plates were coated with 0.5 μg of MOG (35 - 55), PLP (183 - 199), or MBP (83 - 99) (Toray Research Center, Inc., Tokyo, Japan). These peptides were extracellular domains of the naive antigens and were considered epitopes against autoantibodies in demyelinating diseases of the central nervous system [11,12]. An uncoated well was used as a control. After incubation with 1% bovine serum albumin (BSA) in phosphate-buffered saline (PBS), the serum was diluted to 1:40 with 1% BSA in PBS and added to each well; the plate was incubated at room temperature for 2 h. After washing with PBS, peroxidase-conjugated goat anti-human IgG antibody (Jackson ImmunoResearch Laboratories, Inc., West Grove, PA, USA), which was diluted 1:10000 with 1% BSA in PBS, or peroxidase-conjugated goat anti-human IgM (MP Biomedicals LLC, Irvine, CA, USA), which was diluted 1:200 with the same solution, was added to each well. After incubation, the wells were washed and orthophenylenediamine dihydrochloride (40 mg/dL of phosphate-citrate buffer, pH 5.0) was used to obtain a color reaction. The reaction was stopped by the addition of 8 N H_2SO_4, after which the optical density (OD) of each well was read at 490 nm using an ELISA reader (Model 550, Bio-Rad, Hercules, California, USA). Each OD value was corrected by subtracting the OD value of the control well that had been similarly processed. The ELISAs were repeated 3 times, and the mean OD of the 3 experiments was calculated. Sera with corrected OD values that were greater than +3SD of the normal control values were considered positive.

2.3. Statistical Analysis

The differences in the populations were tested by the X^2 test for independence. The F test was used to assess whether the distributions of the data variables were equal among the groups. The two-sample *t* test and the Welch's *t* test were used to compare the differences between groups (anti-myelin antibody-positive and anti-myelin antibody-negative). The Pearson product moment correlation coefficient was used to assess the correlations among the data variables. A two-tailed *P* value of less than 0.05 was considered statistically significant.

3. RESULTS

3.1. Frequencies of Anti-Myelin Antibodies

The mean +3SD values of the corrected OD values of the healthy controls were as follows: 0.131 for the anti-MOG IgM antibody; 0.089 for the anti-PLP IgM antibody; 0.086 for the anti-MBP IgM antibody, 0.041 for the anti-MOG IgG antibody, 0.055 for the anti-PLP IgG antibody, and 0.064 for the anti-MBP IgG antibody. None of the 30 healthy controls or the 63 diseased controls was positive for anti-myelin antibodies. No significant differences in frequency were found among normal and disease controls. In comparison, 5 of the 17 patients with NMO (29%) exhibited at least one of the anti-myelin antibodies ($P < 0.0001$ in a X^2 test). A summary of the patients with antibodies to myelin antigens is shown in **Table 1**.

3.2. Clinical Features of Patients with NMO and Anti-Myelin Antibodies

Patients with NMO were divided into anti-myelin antibody-positive and anti-myelin antibody-negative groups. The clinical features of the patients in each group are presented in **Table 2**. Cerebrospinal fluid (CSF) samples were obtained in order to examine the cell count; the content of IgG was examined on the same day as the serum. Scores on the expanded disability status scale (EDSS) were assessed when the patients' conditions were at their worst.

Since the F test used to test the parameters of the CSF cell count and EDSS did not show an equal distribution of the data variables among the groups, a Welch's *t* test was employed. Since the CSF IgG and attack frequency parameters exhibited an equal distribution, a two-sample *t* test was used.

Table 1. Summary of patients with neuromyelitis optica (NMO) and antibodies to myelin antigens.

Patient	Age (y)/sex	Disease	EDSS	IgM antibodies	IgG antibodies
1	20/F	NMO	6	MOG, PLP	negative
2	60/F	NMO overlapping APS	7	MOG, PLP, MBP	negative
3	52/F	NMO	8.5	negative	MOG, PLP, MBP
4	48/F	NMO	8	negative	PLP, MBP
5	32/F	NMOSD	4.5	MOG	negative

APS, anti-phospholipid antibody syndrome; EDSS, expanded disability status scale; MBP, myelin basic protein; MOG, myelin oligodendrocyte glycoprotein; NMOSD, spectrum disease; PLP, proteolipid protein.

Copyright © 2013 SciRes.

Table 2. Clinical features of patients with NMO with and without anti-myelin antibodies.

Clinical features	Positive (n = 5)	Negative (n = 12)
Age (years)*	42.0 ± 14	53 ± 17
Males: females	0:5	1:11
Brain magnetic resonance imaging		
Number of patients with abnormalities	4 (80%)	8 (67%)
Location	cerebrum, brainstem	cerebrum, brainstem, pons
Optic neuritis	2 (40%)	4 (33%)
Long spinal cord lesion	2 (40%)	8 (67%)
Cerebrospinal fluid (CSF) cell count*†	270 ± 282 (n = 4)	75 ± 149 (n = 10)
CSF IgG*†	8.9 ± 4.8 (n = 4)	9.4 ± 6.1 (n = 10)
expanded disability status scale (EDSS)*‡	6.8 ± 1.4	5.1 ± 3.0
Attack frequency* (per year)	1.86 ± 0.77	1.72 ± 1.28
Number of autoantibodies*	2.80 ± 1.60	0.50 ± 0.96

*mean ± SD; †CSF was obtained on the same day as the serum sample; ‡EDSS were assessed when the condition of the patient was at its worst.

The EDSS scores correlated with the titer of the anti-myelin IgG antibodies, MOG (P = 0.036, R^2 = 0.37), PLP (P = 0.042, R^2 = 0.35) and MBP (P = 0.036, R^2 = 0.37) (**Figure 1**), and the score of all patients with high titers of antibodies against any of the myelin antigens was more than 4.5 (**Table 1**). However, there were no correlations between the EDSS scores and the titers of the following antibodies: anti-MOG IgM (P = 0.76), anti-PLP IgM (P = 0.78), anti-MBP IgM (P = 0.75), anti-MOG IgG (P = 0.57), anti-PLP IgG (P = 0.68), and anti-MBP (P = 0.45).

3.3. Number of Autoantibodies Except for Anti-AQP4 and Anti-Myelin Antibodies

The presence of other autoantibodies was examined in the sera of all patients. The antibodies examined were rheumatoid factor, anti-nuclear antibody, anti-Ro/SS-A antibody, anti-scleroderma-70 antibody, anti-cardiolipin antibody, lupus anticoagulant, thyroid stimulating antibody, anti-thyroid peroxidase antibody, and anti-thyroglobulin antibody. In the negative group, 1 patient had a complication of Sjögren syndrome. In the positive group, 1 patient exhibited anti-phospholipid antibody syndrome (APS), another had subclinical autoimmune thyroidism, and a third patient had a family history of systemic lupus erythematosus (SLE). The patients in the anti-myelin antibody-positive group presented with other autoantibodies more frequently than the negative group patients and this difference was significant (mean ± SD, 2.80 ± 1.60 versus 0.50 ± 0.96, P = 0.037 with Welch's t test).

4. DISCUSSIONS

In this retrospective case-control study, we found that the EDSS scores showed a correlation with the titer of the anti-myelin antibodies and an increase in the frequency of anti-myelin antibodies in patients with NMO. ELISA was chosen to determine the presence of IgM and IgG anti-myelin antibodies since it is easily performed and can quantitatively analyze the titer of antibodies as OD values. All of the patients who were positive for anti-myelin antibodies had NMO or NMO spectrum diseases; none of the patients with conventional MS were positive for anti-myelin antibodies.

This frequency was lower than that found of a prior study that used ELISA to assess the serum level of anti-MOG IgG (rh-MOG 1 - 125) in patients with MS. IgG MOG seropositivity was reported in 22% of patients with MS by Pittock, *et al.* and in 33% of patients with MS by Wang, *et al.* [7,8]. This discrepancy may be due to the MOG-antigen used to coat the ELISA plate. For example, MOG-IgG (1 - 125) might be highly sensitive as an antigen compared to the MOG peptide (35 - 55). Another possible factor is the time-course used to determine the presence of anti-MOG antibodies since some patients who tested seropositive for MOG antibodies became seronegative during the follow-up period. O'Connor, *et al.* revealed that only the anti-MOG antibodies found in MS lesions had a high affinity for their antigens, whereas serum and CSF antibodies to MOG were low-affinity antibodies [12]. This means that the particular MOG antibodies detected could relate to the patterns of demyelination observed in MS.

Several studies have focused on the prognostic value of anti-MOG in the progression of MS in patients with clinical isolated syndrome (CIS). Berger, *et al.* reported that IgM anti-MOG antibodies and MBP antibodies, measured by Western blot, were predictors of MS development in a cohort of 103 patients with CIS [13]. Furthermore, these authors found that healthy young adults with detectable serum levels of IgG anti-MOG antibodies had an increased risk of developing MS. The predictive

Copyright © 2013 SciRes.

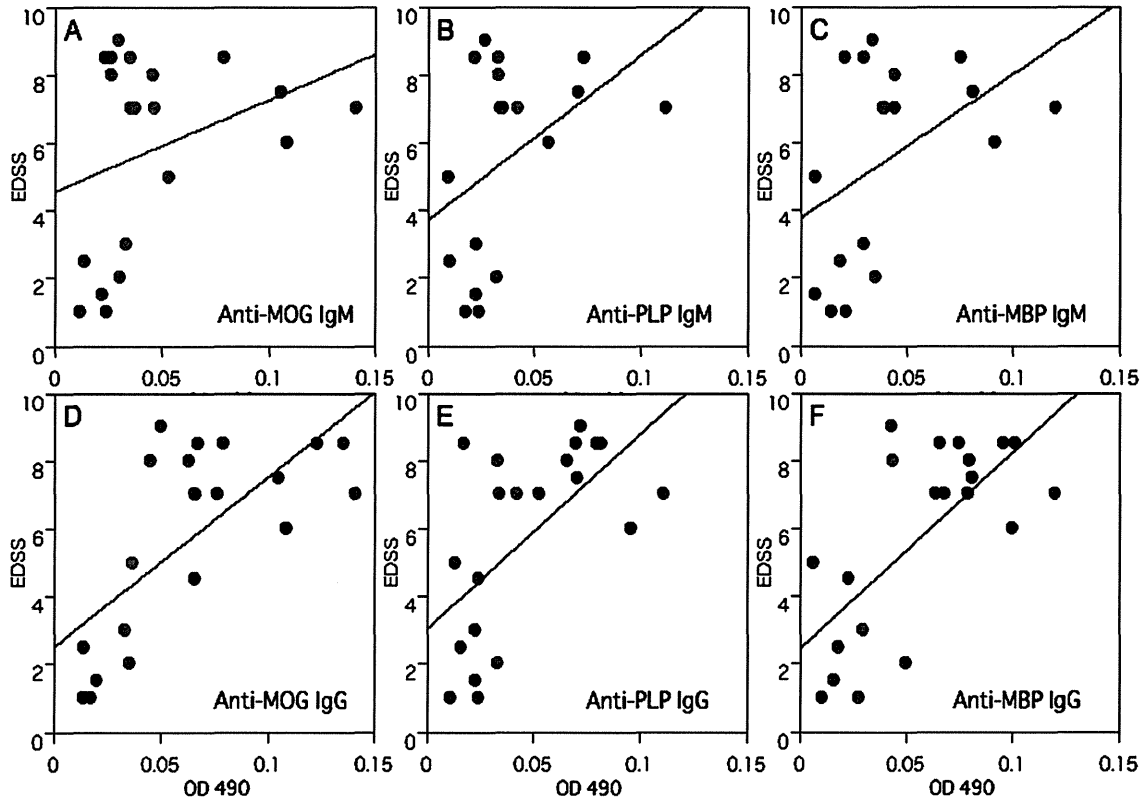

Figure 1. Correlation of the expanded disability status scale (EDSS) scores and the titers of autoantibodies to myelin antigens. The EDSS scores correlated with the titers of the following antibodies: anti-MOG IgG ($P = 0.036$, $R^2 = 0.37$), anti-PLP IgG ($P = 0.042$, $R^2 = 0.35$) and anti-MBP IgG ($P = 0.036$, $R^2 = 0.37$). There were no correlations between the EDSS scores and the titers of the following antibodies: anti-MOG IgM ($P = 0.76$), anti-PLP IgM ($P = 0.78$), anti-MBP IgM ($P = 0.75$), anti-MOG IgG ($P = 0.57$), anti-PLP IgG ($P = 0.68$), and anti-MBP ($P = 0.45$). All patients with high titers of antibodies against myelin antigens scored more than 4.5 on the EDSS.

role of anti-myelin antibodies has been addressed in several different studies with correlations ranging from highly significant [14] to partially significant [15,16] to not significant [17,18]. The different results might reflect discrepancies in study designs and/or study populations.

In patients with NMO, autoantibody responses to the myelin antigens analyzed in this study by ELISA have previously been reported. All patients showed a positive and predominant anti-MOG response rather than an anti-MBP autoantibody response [19]. It has been speculated that anti-MOG antibodies might be involved in the demyelinating process in NMO. To study immunologic alterations, Correale, *et al.* analyzed anti-MOG positive mononuclear cells in peripheral blood and CSF using ELISPOT assays. Their study found that MOG-specific responses in CSF showed significant increases in IgG- and IgM-secreting cells in patients with NMO compared to patients with MS and healthy subjects [20]. These findings are in agreement with observations indicating more severe clinical manifestations in patients with NMO compared to those with MS. In the blood and CSF of patients with NMO, the mean number of IL-6-secreting cells was higher compared to that of MS and healthy control subjects. A strong correlation between the number of cells secreting anti-MOG antibodies and antigen-specific IL-6 synthesis was observed in CSF collected exclusively from patients with NMO [20].

Alves-Leon, *et al.* used ELISA to assess the production of IgG and IgA antibodies to antigens of MBP, PLP (95 - 116), and MOG (92 - 106) in 28 patients with NMO and healthy matched controls. Patients with NMO had significantly higher levels of IgGs to MOG ($P < 0.0001$), PLP ($P = 0.0002$), and MBP ($P < 0.0001$) compared to healthy controls [21]. Those authors suggested that the high expression of MOG (92 - 106), PLP (95 - 116), and MBP autoantibodies in patients with NMO could be a marker for the prognosis, recurrence, and/or severity of the disease.

In our study, the EDSS correlated with the titer of the anti-myelin antibodies. Furthermore, all patients with high titers of antibodies against myelin antigens scored higher than 4.5 points on the EDSS. These results could reflect severe inflammation of the central nervous system and poor prognoses in patients with anti-myelin antibo-

Copyright © 2013 SciRes.

dies. NMO is often associated with several autoantibodies, as well as anti-AQP4 antibodies, and these are also seen in other autoimmune diseases, especially autoimmune thyroidism, SLE, Sjögren syndrome, and APS [22, 23]. The overlap presence of these antibodies with other autoimmune diseases is considered a factor in the prediction of poor prognoses and/or poor responses to treatment, as reported in patients with NMO overlapping with Sjögren syndrome.

Our study revealed that the patients in the anti-myelin antibody-positive group presented with other autoantibodies more frequently than the negative group patients. In the positive group, 2 of 5 patients overlapped with other autoimmune diseases, while 1 patient had a family history of severe SLE.

We could clearly detect an association between the presence of these antibodies and the severity and clinical features of the disease. Our study also revealed increased EDSS scores in patients with high titers of anti-myelin antibodies. As reported in pathological and CSF studies, the demyelination that occurs subsequent to astrocytic damage in NMO is considered to be more severe than that observed in MS [24]. In addition, a recent study reported that anti-AQP4 antibodies damage oligodendrocytes through an excitotoxic mechanism following the disruption of glutamate homeostasis in astrocytes *in vitro* [25]. These findings allowed us to hypothesize that myelin antibodies were produced subsequent to the leakage of myelin antigens due to massive inflammation within the central nervous system.

In conclusion, anti-myelin antibodies in sera, as well as other autoantibodies and overlapping autoimmune diseases, may be useful markers for predicting severe clinical courses or poor prognoses in patients with NMO.

5. ACKNOWLEDGEMENTS

This work was supported in part by the Ministry of Health, Labor and Welfare of Japan (Health and Labor Sciences Research Grants; Research on intractable diseases, H23-017).

REFERENCES

[1] Wingerchuk, D.M. and Weinshenker, B.G. (2003) Neuromyelitis optica: Clinical predictors of a relapsing course and survival. *Neurology*, **60**, 848-853. doi:10.1212/01.WNL.0000049912.02954.2C

[2] Carroll, W.M. and Fujihara, K. (2010) Neuromyelitis optica. *Current Treatment Options in Neurology*, **12**, 244-255. doi:10.1007/s11940-010-0071-z

[3] Marignier, R., Nicolle, A., Watrin, C., *et al.* (2010) Oligodendrocytes are damaged by neuromyelitis optica immunoglobulin G via astrocyte injury. *Brain*, **133**, 2578-2591. doi:10.1093/brain/awq177

[4] Sospedra, M. and Martin, R. (2005) Immunology of multiple sclerosis. *Annual Reviews of Immunology*, **23**, 683-747.doi:10.1146/annurev.immunol.23.021704.115707

[5] Kerlero de Rosbo, N., Honegger, P., Lassmann, H., *et al.* (1990) Demyelination induced in aggregating brain cell cultures by a monoclonal antibody against myelin/oligodendrocyte glycoprotein. *Journal of Neurochemistry*, **55**, 583-587. doi:10.1111/j.1471-4159.1990.tb04173.x

[6] Stefferl, A., Brehm, U., Storch, M., *et al.* (1999) Myelin oligodendrocyte glycoprotein induces experimental autoimmune encephalomyelitis in the resistant. *Journal of Immunology*, **163**, 40-49.

[7] Pittock, S.J., Reindl, M., Achenbach, S., *et al.* (2007) Myelin oligodendrocyte glycoprotein antibodies in pathologically proven multiple sclerosis: Frequency, stability and clinicopathologic correlations. *Multiple Sclerosis Journal*, **13**, 7-16. doi:10.1177/1352458506072189

[8] Wang, H., Munger, K.L., Reindl, M., *et al.* (2008) Myelin oligodendrocyte glycoprotein antibodies and multiple sclerosis in healthy young adults. *Neurology*, **71**, 1142-1146.

[9] Kezuka, T., Usui, Y., Yamakawa, N., *et al.* (2012) Relationship between NMO-antibody and anti-MOG antibody in optic neuritis. *Journal of Neuro-Ophthalmology*, **32**, 107-110. doi:10.1097/WNO.0b013e31823c9b6c

[10] Wingerchuk, D.M., Lennon, V.A., Pittock, S.J., *et al.* (2006) Revised diagnostic criteria for neuromyelitis optica. *Neurology*, **66**, 1485-1489. doi:10.1212/01.wnl.0000216139.44259.74

[11] Johns T.G. and Bernard C.C. (1999) The structure and function of myelin oligodendrocyte glycolprotein. *Journal of Neurochemistry*, **72**, 1-9. doi:10.1111/j.1471-4159.1999.tb11579.x

[12] Khalis, M., Reindl, M., Lutterotti, A., *et al.* (2006) Epitope specificity of serum antibodies directed against the extracellular domain of myelin oligodendrocyte glycolprotein: Influence of relapses and immunomodulatory treatments. *Journal of Neuroimmunology*, **174**, 147-156.

[13] Berger, T., Rubner, P., Schautzer, F., *et al.* (2003) Antimyelin antibodies as a predictor of clinically definitive multiple sclerosis after a first demyelinating event. *The New England Journal of Medicine*, **349**, 139-145. doi:10.1056/NEJMoa022328

[14] Tomassini, V., De Giglio, L., Reindl, M., *et al.* (2007) Anti-myelin antibodies predict the clinical outcome after a first episode suggestive of MS. *Multiple Sclerosis Journal*, **13**, 1086-1094. doi:10.1177/1352458507077622

[15] Rauer, S., Euler, B., Reindl, M. and Berger, T. (2006) Antimyelin antibodies and the risk of relapse in patients with a primary demyelinating event. *Journal of Neurology, Neurosurgery & Psychiatry*, **77**, 739-742. doi:10.1136/jnnp.2005.077784

[16] Kuhle, J., Pohl, C., Mehling, M., *et al.* (2007) Lack of association between antimyelin antibodies and progresssion to multiple sclerosis. *The New England Journal of Medicine*, **356**, 371-378. doi:10.1056/NEJMoa063602

[17] Lim, E.T., Berger, T., Reindl, M., *et al.* (2005) Anti-myelin antibodies do not allow earlier diagnosis of multiple sclerosis. *Multiple Sclerosis*, **11**, 492-494.

Copyright © 2013 SciRes.

[18] Pelayo, R., Tintoré, M., Montalban, X., *et al.* (2007) Anti-myelin antibodies with no progression to multiple sclerosis. *The New England Journal of Medicine*, **356**, 426-428. doi:10.1056/NEJMc062467

[19] Haase, C.G. and Schmidt, S. (2001) Detection of brain-specific autoantibodies to myelin oligodendrocyte glycoprotein, S100β and myelin basic protein in patients with Devic's neuromyelitis optica. *Neuroscience Letters*, **307**, 131-133. doi:10.1016/S0304-3940(01)01949-8

[20] Correale, J. and Fiol, M. (2004) Activation of humoral immunity and eosinophils in neuromyelitis optica. *Neurology*, **63**, 2363-2370. doi:10.1212/01.WNL.0000148481.80152.BF

[21] Alves-Leon, S.V., Pimentel, M.L., Sant'Anna, G., *et al.* (2008) Immune system markers of neuroinflammation in patients with clinical diagnose of neuromyelitis optica. *Arquivos de Neuro-Psiquiatr*, **66**, 678-684. doi:10.1590/S0004-282X2008000500013

[22] Kahlenberg, J.M. (2011) Neuromyelitis optica spectrum disorder as an initial presentation of primary Sjögren's syndrome. *Seminars in Arthritis and Rheumatism*, **40**, 343-348. doi:10.1016/j.semarthrit.2010.05.005

[23] Pittock, S.J., Lennon, V.A., De Seze, J., *et al.* (2008) Neuromyelitis optica and non-organ-specific autoimmunity. *Archives of Neurology*, **65**, 78-83. doi:10.1001/archneurol.2007.17

[24] Takano, R., Misu, T., Takahashi, T., *et al.* (2010) Astrocytic damage is far more severe than demyelination in NMO. *Neurology*, **75**, 208-216. doi:10.1212/WNL.0b013e3181e2414b

[25] Marignier, R., Giraudon, P., Vukusic, S., *et al.* (2010) Anti-aquaporin-4 antibodies in Devic's neuromyelitis optica: Therapeutic implications. *Therapeutic Advances in Neurological Disorders*, **3**, 311-321. doi:10.1177/1756285610382478

Copyright © 2013 SciRes.

Research Paper

MULTIPLE SCLEROSIS JOURNAL | MSJ

Multiple Sclerosis Journal
0(0) 1–11
© The Author(s) 2013
Reprints and permissions:
sagepub.co.uk/journalsPermissions.nav
DOI: 10.1177/1352458512471873
msj.sagepub.com
SAGE

Molecular network of chromatin immunoprecipitation followed by deep sequencing-based vitamin D receptor target genes

Jun-ichi Satoh and Hiroko Tabunoki

Abstract

Background: Vitamin D is a liposoluble vitamin essential for calcium metabolism. The ligand-bound vitamin D receptor (VDR), heterodimerized with retinoid X receptor, interacts with vitamin D response elements (VDREs) to regulate gene expression. Vitamin D deficiency due to insufficient sunlight exposure confers an increased risk for multiple sclerosis (MS).
Objective: To study a protective role of vitamin D in multiple sclerosis (MS), it is important to characterize the global molecular network of VDR target genes (VDRTGs) in immune cells.
Methods: We identified genome-wide VDRTGs collectively from two distinct chromatin immunoprecipitation followed by deep sequencing (ChIP-Seq) datasets of VDR-binding sites derived from calcitriol-treated human cells of B cell and monocyte origins. We mapped short reads of next generation sequencing (NGS) data on hg19 with Bowtie, detected the peaks with Model-based Analysis of ChIP-Seq (MACS), and identified genomic locations by GenomeJack, a novel genome viewer for NGS platforms.
Results: We found 2997 stringent peaks distributed on protein-coding genes, chiefly located in the promoter and the intron on VDRE DR3 sequences. However, the corresponding transcriptome data verified calcitriol-induced upregulation of only a small set of VDRTGs. The molecular network of 1541 calcitriol-responsive VDRTGs showed a significant relationship with leukocyte transendothelial migration, Fcγ receptor-mediated phagocytosis, and transcriptional regulation by VDR, suggesting a pivotal role of genome-wide VDRTGs in immune regulation.
Conclusion: These results suggest the working hypothesis that persistent deficiency of vitamin D might perturb the complex network of VDRTGs in immune cells, being responsible for induction of an autoimmune response causative for MS.

Keywords

ChIP-Seq, GenomeJack, multiple sclerosis, pathway analysis, vitamin D,VDR

Date received: 4th June 2012; revised: 21st November 2012; accepted: 28th November 2012

Introduction

Multiple sclerosis (MS) is an inflammatory demyelinating disease of the central nervous system (CNS) presenting with relapsing–remitting and progressive clinical courses. Pathologically, it is characterized by inflammation, demyelination, gliosis, and axonal degeneration, although underlying molecular mechanisms remain largely unknown. Even genetically identical monozygotic twins express a concordance rate of approximately 30% for MS. This suggests a great contribution of environmental factors to MS pathogenesis, such as cigarette smoking, Epstein Barr virus (EBV) infection, and low serum vitamin D levels.[1]

Vitamin D is a liposoluble vitamin essential for calcium metabolism, available from dietary sources and also produced endogenously when the sunlight Ultraviolet B (UVB) triggers its synthesis in the skin, followed by consecutive hydroxylation in the liver and kidney to generate 1α,25-dihydroxyvitamin D3, a biologically active form named calcitriol. The vitamin D receptor (VDR) is expressed on various cells including immune cells, such as lymphocytes, macrophages, monocytes, and dendritic cells.

Department of Bioinformatics and Molecular Neuropathology, Meiji Pharmaceutical University, Japan.

Corresponding author:
Jun-ichi Satoh, Department of Bioinformatics and Molecular Neuropathology, Meiji Pharmaceutical University, 2-522-1 Noshio, Kiyose, Tokyo 204-8588, Japan.
Email: satoj@my-pharm.ac.jp

Downloaded from msj.sagepub.com at National Center of Neurology and Psychiatry on February 12, 2013

The ligand-bound VDR, heterodimerized with retinoid X receptor (RXR), interacts with vitamin D response elements (VDREs) on regulatory regions of target genes, and recruits protein complexes that alter chromatin structure. They regulate expression of more than 900 vitamin D-responsive genes involved in calcium homeostasis, cell growth, differentiation, apoptosis, and modulation of immune response.[2] Importantly, the expression of the gene encoding MS-associated MHC class II allele HLA-DRB1*1501 is directly regulated by vitamin D via a VDRE on its promoter.[3]

A prospective case-control study on millions of US military personnel indicated that MS risk is decreased with increasing serum levels of 25-hydroxyvitamin D among white subjects.[4] Higher serum levels of 25-hydroxyvitamin D are associated with a greater suppressive capacity of regulatory T (Treg) cells in relapsing-remitting MS patients.[5] Calcitriol inhibits production of proinflammatory cytokines, such as IFNγ, IL-17, and IL-21, from human $CD4^+$ T cells, being responsible for the anti-inflammatory activity of vitamin D.[6] All of these observations support a protective role of vitamin D in immune cells against development of MS.[7] To elucidate underlying molecular mechanisms, it is important to characterize the global molecular network of VDR target genes (VDRTGs) presenting with diverse biological roles in immune cells, including those previously underestimated in immunopathogenesis of MS.

Recently, the rapid progress in the next-generation sequencing (NGS) technology has revolutionized the field of genome research. Notably, NGS thoroughly characterized the genetic basis of MS at the level of the whole genome of individual patients.[8] Chromatin immunoprecipitation followed by deep sequencing (ChIP-Seq) has been used as a NGS application to achieve genome-wide profiling of DNA-binding proteins, histone modifications, and nucleosomes.[9] ChIP-Seq with an advantage of higher resolution, less noise, and greater coverage of the genome, compared with the microarray-based ChIP-Chip method, and provides an innovative tool for studying the comprehensive gene regulatory networks. Since NGS analysis produces extremely high throughput experimental data, it is often difficult to extract the biologically meaningful implications. Recent advances in systems biology enable us to illustrate the cell-wide map of the complex molecular interactions by using the literature-based knowledgebase of molecular pathways.[10] The logically-arranged molecular networks construct the whole system, characterized by robustness, which maintains the proper function of the system in the face of genetic and environmental perturbations. Therefore, the integration of high-dimensional NGS data with underlying molecular networks serves as a rational approach to characterize the genome-wide network-based molecular mechanisms of gene regulation.

For an initial step to study molecular mechanisms underlying vitamin D-mediated protection against MS, we identified thousands of *in vivo* calcitriol-responsive VDRTG candidates collected from two public ChIP-Seq datasets of VDR-binding sites in human cells of B cell and monocyte origins, and investigated their molecular network by using three distinct pathway analysis tools of bioinformatics. We focused on the datasets derived from immune-relevant cell types of B cell and monocyte origins because B cells and monocytes play a key role in MS pathogenesis by serving as a source of proinflammatory and immunoregulatory cytokines and chemokines.[11]

Datasets and methods

Two distinct ChIP-Seq datasets of VDR-binding sites

We identified a comprehensive set of VDRTGs from two distinct ChIP-Seq datasets of VDR-binding sites numbered SRP002673 and SRP005910, retrieved from DDBJ Sequence Read Archive (DRA) (trace.ddbj.nig.ac.jp/DRASearch). SRP002673 contained the dataset of EBV-transformed human B lymphoblast cell lines (LCLs) isolated from two Centre d'Etude du Polymorphisme Humain (CEPH) individuals GM10855 and GM10861 who participated in the HapMap project.[12] The cells were treated with or without 100 nM calcitriol for 36 h, and then processed for ChIP-Seq using a rabbit anti-VDR antibody (sc-1008; Santa Cruz Biotechnology, USA). They were processed in parallel for transcriptome analysis on a Human Gene 1.0 ST Array (Affymetrix). We retrieved the transcriptome dataset numbered GSE22176 from Gene Expression Omnibus (GEO) (www.ncbi.nlm.nih.gov/gds). SRP005910 contained the dataset of THP-1 human monocyte leukemia cell line following exposure to 10 nM calcitriol or vehicle (ethanol) for 40 min for ChIP-Seq with a rabbit anti-VDR antibody (ab3508; Abcam) and for 4 h for transcriptome analysis on a Human-6 v2.0 Expression Beadchip (Illumina, San Diego, California, USA).[13] We retrieved the transcriptome dataset numbered GSE27270 from GEO. ChIP DNA fragments were processed for deep sequencing at a 35 bp (SRP002673) or a 36 bp (SRP005910) read length on the Genome Analyzer II (Illumina).

We mapped short reads of NGS data on the human genome reference sequence numbered hg19 by using Bowtie 0.12.7 (bowtie-bio.sourceforge.net). Then, we detected the statistically significant peaks of mapped reads by using Model-based Analysis of ChIP-Seq (MACS; liulab.dfci.harvard.edu/MACS) under the stringent condition of fold enrichment (FE)≥20 and the false discovery rate (FDR)≤1%. Finally, we identified genomic locations of the peaks by importing the processed data into GenomeJack v1.3, a novel genome viewer for NGS platforms (Mitsubishi Space Software; www.mss.co.jp/businessfield/bioinformatics). Based on RefSeq ID, the MACS peaks were categorized into those located on protein-coding genes with mRNA-

Downloaded from msj.sagepub.com at National Center of Neurology and Psychiatry on February 12, 2013

coding transcript (NM)-heading numbers, those on non-coding genes with non-coding transcript (NR)-heading numbers, and those located in intergenic regions without relevant neighboring genes. Since proximal promoters are generally located within several hundreds bp upstream of the transcription start site (TSS), the genomic locations of the summits were classified into the promoter region defined by the location within a 5 kb upstream from the 5' end of genes, the 5' untranslated region (5'UTR), the exon, the intron, and the 3'UTR. The locations outside these, which might include the locations of several distal promoters, were tentatively defined as intergenic regions, owing to the inability to accurately assess relevant target genes. The consensus motif sequences were identified by importing a 400 bp-length sequence surrounding the peak summit into MEME-ChIP (meme.sdsc.edu/meme/cgi-bin/meme-chip.cgi).

We also analyzed the transcriptome data of microarray analysis corresponding to the ChIP-Seq datasets. The log2-converted normalized data were evaluated by Welch's t-test to identify the genes differentially expressed between calcitriol-treated and control samples.

Molecular network analysis

To identify biologically relevant molecular networks and pathways, we imported Entrez Gene IDs of VDRTGs into the Functional Annotation tool of Database for Annotation, Visualization and Integrated Discovery (DAVID) v6.7 (david.abcc.ncifcrf.gov). DAVID identifies the most relevant pathway constructed by Kyoto Encyclopedia of Genes and Genomes (KEGG) (www.kegg.jp), composed of the genes enriched in the given set with an output of statistical significance evaluated by the modified Fisher's exact test. KEGG is a publicly accessible knowledgebase containing manually curated reference pathways that cover a wide range of metabolic, genetic and cellular processes, and human diseases, currently composed of 218,213 pathways generated from 435 reference pathways. We also imported Entrez Gene IDs into Ingenuity Pathways Analysis (IPA) (Ingenuity Systems; www.ingenuity.com) and KeyMolnet (Institute of Medicinal Molecular Design; www.immd.co.jp), both of which are commercial tools for molecular network analysis.

IPA is a knowledgebase that contains approximately 2,500,000 biological and chemical interactions and functional annotations with definite scientific evidence. By uploading the list of Gene IDs and expression values, the network-generation algorithm identifies focused genes integrated in a global molecular network. IPA calculates the score p-value, the statistical significance of association between the genes and the networks by the Fisher's exact test.

KeyMolnet contains knowledge-based contents on 150,500 relationships among human genes and proteins, small molecules, diseases, pathways and drugs.[10] They are categorized into the core contents collected from selected review articles with the highest reliability or the secondary contents extracted from abstracts of PubMed and Human Reference Protein database (HPRD). By importing the list of Gene IDs and expression values, the neighboring network-search algorithm selected one or more molecules as starting points to generate the network of all kinds of molecular interactions around starting molecules, including direct activation/inactivation, transcriptional activation/repression, and the complex formation within the designated number of paths from starting points. The generated network was compared side by side with 484 human canonical pathways of the KeyMolnet library. The algorithm counting the number of overlapping molecular relations between the extracted network and the canonical pathway makes it possible to identify the canonical pathway showing the most significant contribution to the extracted network.

Results

Identification of 2997 VDR target genes from two distinct ChIP-Seq datasets

By analyzing two distinct VDR-binding ChIP-Seq datasets numbered SRP002673 and SRP005910, derived from three samples of calcitriol-treated cells and three samples of non-treated or vehicle-treated (control) cells, we identified totally 4718 stringent ChIP-Seq peaks showing FE≥20 and FDR≤1% (Table 1). The genomic locations of the peaks were determined by using GenomeJack (Figure 1(a)). VDRE consensus sequences, comprising direct or inverted repeats of hexameric (G/A)G(G/T)TCA motifs with three intervening base pairs (DR3), were detected in the top 50 enriched genes in calcitriol-treated samples (Figure 1(b); Figure 2). After omitting the peaks located on non-coding genes and those located in intergenic regions, we identified 2997 peaks located on protein-coding genes that have their summits on the promoter (n=1353), 5'UTR (n=249), exon (n=85), intron (n=1253) or 3'UTR (n=57) (Table 1; Supplementary Tables 1–3 online). They are tentatively designated as ChIP-Seq-based VDRTGs.

Calcitriol-induced upregulation of a small set of ChIP-Seq-based VDR target genes

We also analyzed the transcriptome data numbered GSE22176 and GSE27270 corresponding to the ChIP-Seq datasets. Initially, we could not detect any genes differentially expressed between calcitriol-treated and control samples by the microarray-standard statistical evaluation with Welch's t-test followed by Bonferroni correction for multiple comparison, except for CD14 exhibiting a 6.65-fold increase in THP-1 cells by calcitriol treatment (p=0.0000004). Therefore, we attempted to extract greater numbers of calcitriol-responsive genes under the statistically less stringent condition of p≤0.05 by Welch's t-test

Downloaded from msj.sagepub.com at National Center of Neurology and Psychiatry on February 12, 2013

Table 1. The overview of vitamin D receptor (VDR) target genes with stringent chromatin immunoprecipitation followed by deep sequencing (ChIP-Seq) peaks.

Datasets	Samples and treatment	Peaks on coding genes	Location of summits on coding genes					Peaks on non-coding genes	Peaks on intergenic regions	Total numbers of peaks
			Promoter	5'UTR	Exon	Intron	3'UTR			
SRP002673	**GM10855LCL-control**	54	39	8	1	5	1	8	6	68
	GM10855LCL-calcitriol	200	54	7	4	126	9	23	118	341
	GM10861LCL-control	402	281	63	7	48	3	41	70	513
	GM10861LCL-calcitriol	2047	875	161	50	919	42	223	1020	3290
SRP005910	**THP1-control**	108	55	5	14	34	0	15	63	186
	THP1-calcitriol	186	49	5	9	121	2	17	117	320
Total numbers of peaks		2997	1353	249	85	1253	57	327	1394	4718

By analyzing two distinct ChIP-Seq datasets of VDR-binding sites numbered SRP002673 and SRP005910, composed of three calcitriol-treated and three non-treated or vehicle-treated (control) samples, we identified stringent peaks exhibiting fold enrichment (FE)≥20 and false discovery rate (FDR)≤1%, which were categorized into the summits of the peaks located on protein-coding genes, those on non-coding genes and those in intergenic regions, by using GenomeJack.

without adjustment by Bonferroni correction and fold change ≥1.5 as upregulation or ≤0.75 as downreguation. This evaluation results in detection of overall 134 upregulated and 43 downregulated genes (Supplementary Tables 4–6 online). The set of 29 genes (21.6%) among 134 upregulated genes agreed with ChIP-Seq-based VDRTGs, including CLMN, PPP1R2, SPATA13, SULF2, P2RY8, MOBKL2B, CAMP, CD38, FAM116B, SERINC2, TRIM31, SLC25A20, TNFRSF17, ALDH1A1, CTSZ, ASAP2, SLC37A2, LRRC8A, TMEM37, C20orf197, PDZD7, SFXN3, PRKCH, SEMA4D, SEMA6B, CYTH4, ITGB5, ELF4, and ZMIZ1. In contrast, none of the downregulated genes have met with the list of ChIP-Seq-based VDRTGs.

Identification of 1541 ChIP-Seq-based calcitriol-responsive VDR target genes

Next, we combined all VDRTGs derived from three different calcitriol-treated samples into one, named the treatment set composed of 2432 genes, and those from three non-treated samples into one, named the non-treatment set composed of 564 genes. Thus, we found the constitutive binding of VDR on a genome-wide scale to a substantial number of genes in the absence of calcitriol treatment. Then, we extracted a non-redundant set of 1541 calcitriol-responsive genes that were detected exclusively in the treatment set (Supplementary Table 7 online).

Molecular network of 1541 calcitriol-responsive VDR target genes

By importing Entrez Gene IDs of 1541 calcitriol-responsive VDRTGs into the Functional Annotation tool of DAVID, we identified the top five most relevant KEGG pathways (Table 2). They include the pathways in cancer (hsa05200; p=4.92E–05), leukocyte transendothelial migration (hsa04670; p=1.17E–04) (Figure 3), systemic lupus erythematosus (hsa05322; p=5.57E–04), focal adhesion (hsa04510; p=7.30E–04), and Fcγ receptor-mediated phagocytosis (hsa04666; p=2.39E–03).

By using the Core Analysis tool of IPA, we identified the top five most relevant canonical pathways (Supplementary Table 8 online). They include Fcγ receptor-mediated phagocytosis in macrophages and monocytes (p=6.85E–07), molecular mechanisms of cancer (p=1.53E–06), macropinocytosis signaling (p=5.61E–06), glioma signaling (p=1.44E–05), and leukocyte extravasation signaling (p=2.03E–05). Thus, the results of KEGG and IPA showed a substantial overlap between the pathways constructed by VDRTGs, particularly whose function was involved in extravasation and phagocytosis of immune cells. IPA also extracted the top five most relevant functional networks. They include "Gene Expression, Protein Synthesis, Cellular Assembly and Organization" (p=1.00E–126), "Gene Expression, Cancer, Cardiovascular System Development and Function" (p=1.00E–116), "Cellular Function and Maintenance, Protein Degradation, Protein Synthesis" (p=1.00E–92), "Hematological System Development and Function, Tissue Morphology, Humoral Immune Response" (p=1.00E–88), and "Gene Expression, Cellular Development, Tissue Development" (p=1.00E–74) (Supplementary Table 9 online). Importantly, VDR serves as a hub molecule, on which the molecular connections are concentrated, in the functional network defined by "Gene Expression, Cellular Development, Tissue Development" (Figure 4).

Downloaded from msj.sagepub.com at National Center of Neurology and Psychiatry on February 12, 2013

Figure 1. Identification of genomic locations of chromatin immunoprecipitation followed by deep sequencing (ChIP-Seq) peaks by GenomeJack.

By analyzing ChIP-Seq datasets of VDR-binding sites numbered SRP002673 and SRP005910, derived from 3 calcitriol-treated and 3 control samples, we identified totally 4718 peaks showing fold enrichment ≥ 20 and FDR ≤ 1% (Table 1). The genomic locations of the peaks were determined by importing the processed data into GenomeJack. An example of a vitamin D receptor (VDR) target gene named cathelicidin antimicrobial peptide (CAMP) (NM_004345) is shown, where a Model-based Analysis of ChIP-Seq (MACS) peak is located on the promoter region (a) with a vitamin D response element (VDRE) consensus sequence highlighted by orange (b). CAMP has been identified as a target gene for 1α,25-dihydroxyvitamin D3.[34]

By using KeyMolnet, the neighboring network search algorithm extracted a highly complex network, composed of 3300 molecules and 5569 molecular relations. The network exhibited a significant relationship with transcriptional regulation by retinoblastoma protein (Rb)/E2F family proteins (p=1.65E–182), transcriptional regulation by VDR (p=2.74E–171), transcriptional regulation by interferon regulatory factor (IRF) proteins (p=7.03E–103), heat shock protein 90 (HSP90) signaling pathway (p=9.33E–87), and histone acetyltransferase (HAT) signaling pathway (p=3.04E–79). Again, VDR plays a central role in homeostasis of the complex molecular network constructed by VDRTGs (Supplementary Figure 1 online).

Discussion

By using different antibodies, two distinct ChIP-Seq studies numbered SRP002673 and SRP005910 in human immune cells exposed to calcitriol identified 2776 and 2340 VDR-binding sites, respectively.[12,13] They utilized the similar mapping (Bowtie) and peak finding (MACS; FDR<1%) programs. Regardless of great variation of genetic and epigenetic regulation in distinct cell types,[14]

Downloaded from msj.sagepub.com at National Center of Neurology and Psychiatry on February 12, 2013

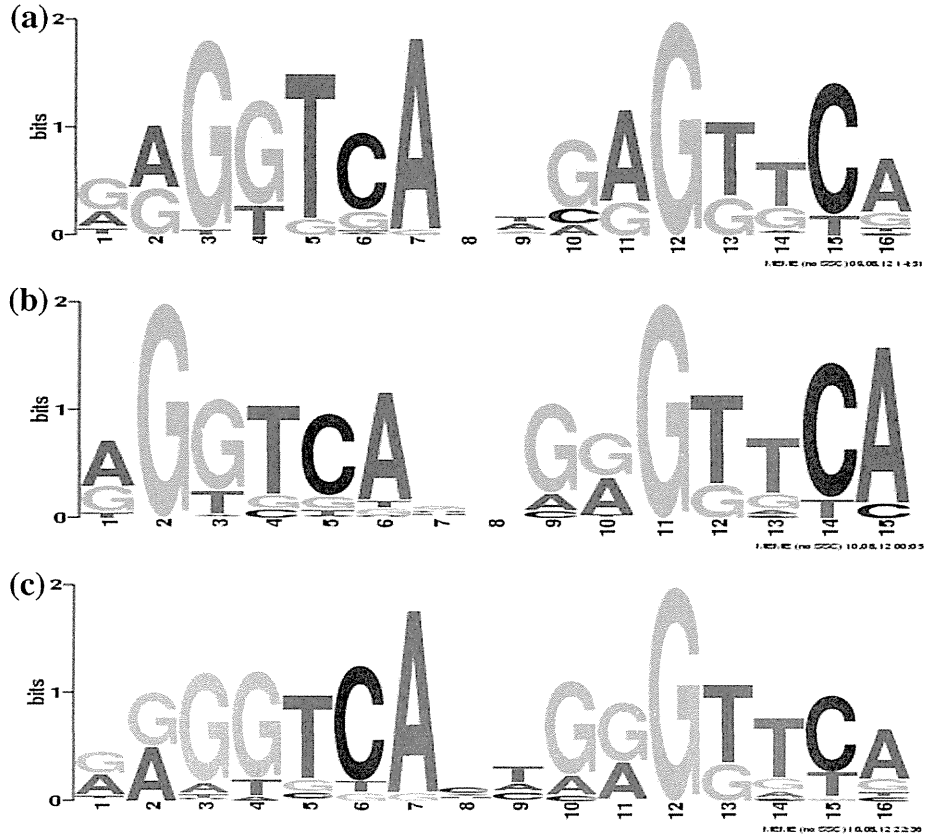

Figure 2. Motif analysis of vitamin D response element (VDRE) consensus sequences on chromatin immunoprecipitation followed by deep sequencing (ChIP-Seq) peaks. The consensus motif sequences were identified by importing a 400 bp-length sequence surrounding the summit of Model-based Analysis of ChIP-Seq (MACS) peaks of the top 50 enriched genes into the MEME-ChIP program. The direct repeats of hexameric (G/A)G(G/T)TCA motifs with three intervening base pairs (DR3) are found in calcitriol-treated samples of (a) GM10855, (b) GM10861, and (c) THP-1 cells.

Table 2. Top five Kyoto Encyclopedia of Genes and Genomes (KEGG) pathways relevant to 1541 calcitriol-responsive vitamin D receptor (VDR) target genes.

KEGG pathway	Molecules in pathway	*p*-value
hsa05200: pathways in cancer	ACVR1B, BCL2, BCL2L1, RUNX1, CDC42, CDK6, COL4A2, CRK, CTBP1, CTNNA1, CTNNB1, E2F2, MECOM, FGF14, GLI3, GRB2, GSK3B, HSP90AB1, ITGA3, LAMA3, LAMA5, LAMB3, LAMC1, MDM2, MSH3, NFKBIA, PDGFA, PLCG1, PLCG2, PRKCA, MAP2K1, PTCH1, PTEN, PTK2, RAC2, RAC3, RXRB, TCF7, TGFB1, HSP90B1, VEGFA, WNT8B, FGF17, TRAF4, PIK3R5, CTNNA3, WNT4, WNT10A, RASSF5, EGLN2	4.92E-05
hsa04670: leukocyte transendothelial migration	RHOH, CDC42, CTNNA1, CTNNB1, CYBA, GRLF1, ICAM1, ITGAL, ITGB2, CD99, NCF4, PLCG1, PLCG2, PRKCA, PTK2, RAC2, RAP1A, VAV1, VAV3, RAPGEF4, PIK3R5, CTNNA3, RASSF5, ESAM	1.17E-04
hsa05322: systemic lupus erythematosus	CD28, CD86, HIST1H2AE, HIST1H2AD, HIST1H2BD, HIST1H2BB, SNRPD3, HIST1H4I, HIST1H2AC, HIST2H2AA3, HIST2H2AC, HIST1H2BG, HIST1H2BL, HIST1H2BM, HIST1H2BF, HIST1H2BI, HIST1H2BO, HIST2H2BE, HIST1H3D, HIST1H4D, HIST1H4K, HIST1H4J, HIST1H4C, HIST1H4H, HIST1H4B, HIST1H4E, HIST2H4A, HIST1H2BJ, HIST1H2AH, HIST1H2BK, HIST2H3C, HIST2H3A, HIST2H2BF HIST2H2AA4	5.57E-04
hsa04510: focal adhesion	BCL2, CDC42, COL4A2, COL6A3, CRK, CTNNB1, GRB2, GRLF1, GSK3B, TNC, ITGA3, ITGB5, LAMA3, LAMA5, LAMB3, LAMC1, PDGFA, PPP1CA, PRKCA, MAP2K1, PTEN, PTK2, RAC2, RAC3, RAP1A, RASGRF1, SRC, VAV1, VEGFA, VAV3, PIK3R5, PDGFD	7.30E-04
hsa04666: Fc gamma R-mediated phagocytosis	CDC42, CRK, INPP5D, PLCG1, PLCG2, PRKCA, PRKCD, PRKCE, MAP2K1, RAC2, VAV1, PIP5K1B, PPAP2C, ASAP2, ARPC2, VAV3, PIK3R5, ARPC5L	2.39E-03

By importing Entrez Gene IDs of 1541 calcitriol-responsive VDR target genes into the Functional Annotation tool of Database for Annotation, Visualization and Integrated Discovery (DAVID), the top five most relevant KEGG pathways were identified. The *p*-value represents statistical significance evaluated by the modified Fisher's exact test.

Downloaded from msj.sagepub.com at National Center of Neurology and Psychiatry on February 12, 2013

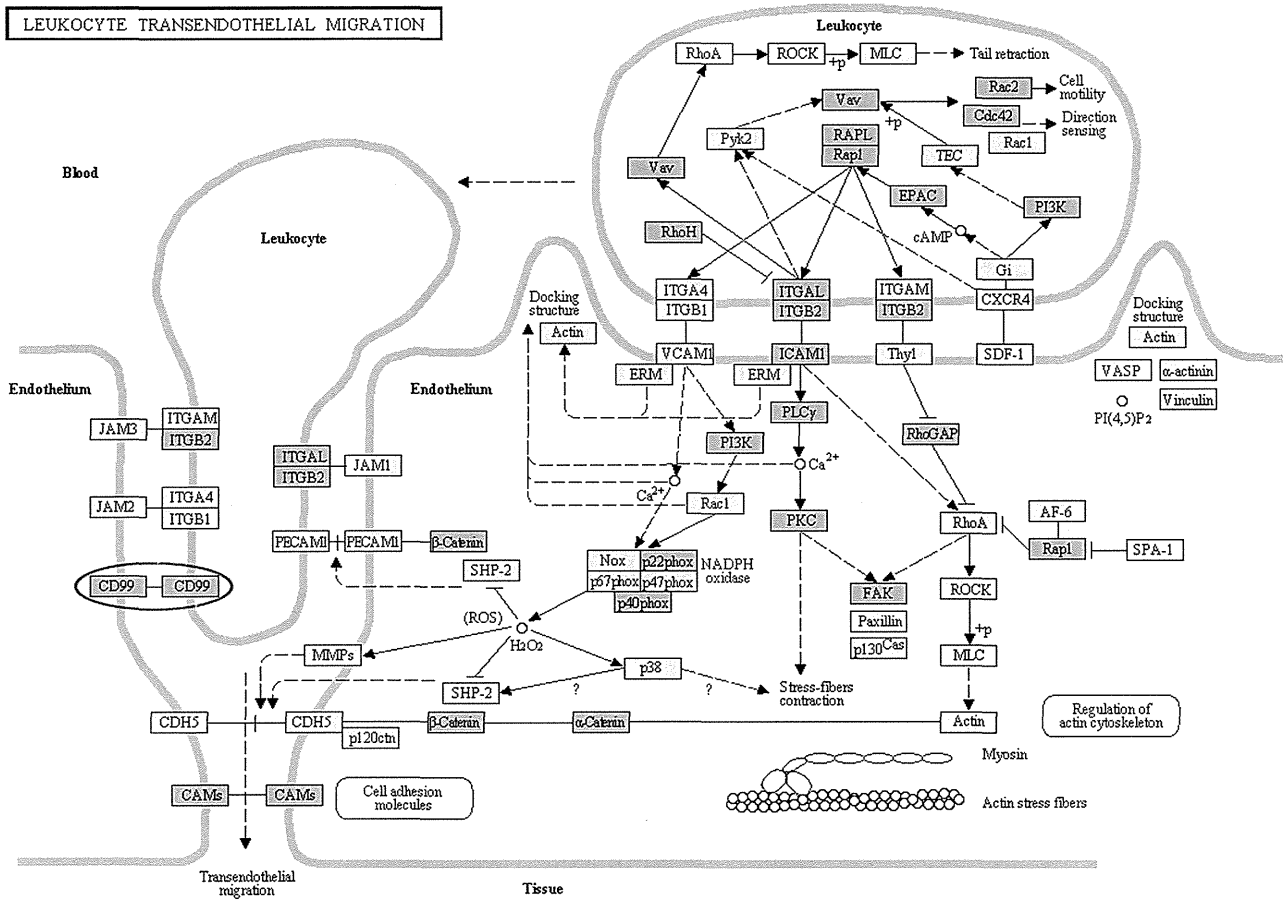

Figure 3. Molecular network of chromatin immunoprecipitation followed by deep sequencing (ChIP-Seq)-based vitamin D receptor (VDR) target genes by Kyoto Encyclopedia of Genes and Genomes (KEGG). The second rank relevant pathway defined by "leukocyte transendothelial migration (hsa04670)" is shown, where VDR target genes (VDRTGs) are colored by orange. CD99, a cell-surface glycoprotein involved in T cell migration and apoptosis, is encircled by a blue ellipse.

VDR-binding sites showed a considerable overlap (18.2%) between the cells originated from B cells and monocytes.[15] However, these studies did not clarify the global molecular network of genome-wide VDRTGs, with respect to immunomodulatory function of vitamin D potentially involved in protection against the development of MS. The ChIP-Seq analysis of VDR target genes derived from lymphocytes of MS patients appears to be preferable, if they are available. As an alternative, we reanalyzed the publicly available datasets of two immune-relevant cells, the cells of B cell and monocyte origins, and combined the results of both to retrieve *in vivo* VDRTG candidates as much as possible.

Although ChIP-Seq serves as a highly efficient method for genome-wide profiling of DNA-binding proteins, it requires some technical considerations:[16] the specificity of the antibody, reproducibility of the results, sequencing depth, and the source of controls, along with cell types, developmental stages, and culture conditions capable of affecting epigenetic features, constitute critical factors. In general, DNA-binding of transcription factors is a highly dynamic process. However, the ChIP-Seq data reflect a snapshot of binding actions. Motif analysis of a defined set of high-quality peaks makes it possible to evaluate the antibody specificity to some extent.[16] We identified VDRE consensus sequences around ChIP-Seq peak summits of all three calcitriol-treated samples, supporting the validity of the experiments. It is not unusual that some biologically important sites show fairly weak ChIP-Seq signals, whereas some sites with very high signals fail to give positive functional output in follow-up experiments.[16] We identified overall 2997 stringent ChIP-Seq peaks located on protein-coding genes. However, by transcriptome analysis, only 20% of upregulated genes and none of downregulated genes in calcitriol-treated cells agreed with ChIP-Seq-based VDRTGs. Most importantly, the molecular network of 1541 calcitriol-responsive VDRTGs is closely related to leukocyte transendothelial migration, Fcγ receptor-mediated phagocytosis, and transcriptional regulation by VDR, suggesting a pivotal role of VDRTGs in immune regulation.

The ligand-bound VDR, heterodimerized with RXR, interacts with VDRE sequences on regulatory regions of target genes.[2] VDR binding to VDREs is ligand-dependent,

Downloaded from msj.sagepub.com at National Center of Neurology and Psychiatry on February 12, 2013

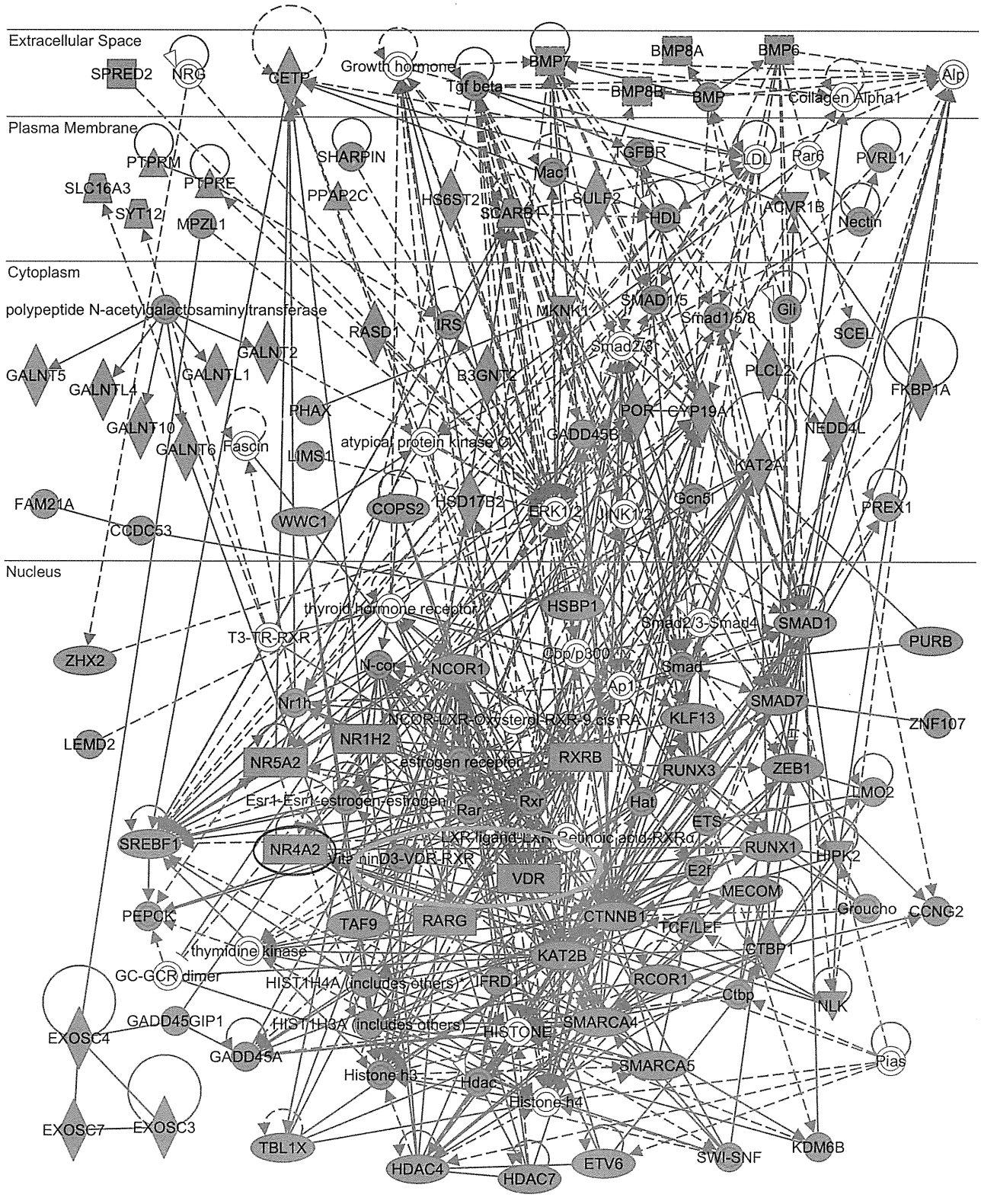

Figure 4. Molecular network of chromatin immunoprecipitation followed by deep sequencing (ChIP-Seq)-based vitamin D receptor (VDR) target genes by Ingenuity Pathways Analysis (IPA). By importing Entrez Gene IDs of the set of 1541 calcitriol-responsive VDR target genes (VDRTGs) into the Core Analysis tool of IPA, we identified the top five most relevant functional networks (Supplementary Table 9 online). The fifth rank relevant network defined by "Gene Expression, Cellular Development, Tissue Development" is shown, where VDRTGs are colored by red. VDR and VDR/ retinoid X receptor (RXR) complex are highlighted by an orange ellipse, while NR4A2, a nuclear orphan receptor involved in differentiation of Th1, Th17, and Treg cells, is encircled by a blue ellipse.

Downloaded from msj.sagepub.com at National Center of Neurology and Psychiatry on February 12, 2013

while RXR binding is ligand-independent.[17] VDREs are often multiple, composed of a pair of hexameric binding sites arranged as direct or inverted repeats interspaced by typically three (DR3) but a varying number of nucleotides different in the context of target genes.[18] We identified 2997 VDR-binding ChIP-Seq peaks distributed on protein-coding genes with location of the summits on the promoter (45.1%), 5'UTR (8.3%), exon (2.8%), intron (41.8%) or 3'UTR (1.9%). Thus, the peaks were concentrated in the promoter and intronic regions having VDRE motifs. The accumulation of VDREs in introns of VDR target genes is not unusual, because VDR-binding sites are located at a frequency of 44% within introns and exons but at only 13% in classical promoter regions in mouse preosteoblasts.[19] Furthermore, VDRE sequences are located occasionally in distant intergenic regions far from target gene promoters.[20] Upon binding to VDRE, the VDR-RXR heterodimer recruits protein complexes that alter the chromatin structure, either open for transcriptional activation or closed for transcriptional repression.[21] For transcriptional activation of target genes, the complex is comprised of CBP/p300 and SRC1 that exhibit histone acetyltransferase (HAT) activity, accompanied by accumulation of ATP-dependent chromatin remodeling complex. For transcriptional repression, the VDR-RXR heterodimer, capable of interfering with cognate transcription factors for expression of their target genes, recruits co-repressors, such as NCOR1, NCOR2, and COPS2, resulting in accumulation of histone deacetylases (HDAC) and DNA methyltransferases (DMT). However, by transcriptome analysis, we did not detect calcitriol-repressed genes having ChIP-Seq-based stringent VDR-binding sites. A recent study suggests that long-term binding is coupled to transcriptional activation, whereas fast binding and turnover is linked to lower levels of transcriptional output, indicating a pivotal role of transcriptional factor-binding dynamics across the genome for fine tuning of expression levels.[22]

The original ChIP-Seq studies of VDR-binding sites corresponding to the datasets we analyzed are quite different in the concentration and exposure time of calcitriol, i.e. B lymphoblast cell lines with 100 nM calcitriol for 36 h[12] versus THP-1 monocyte cell lines with 10 nM calcitriol for 40 min.[13] However, both studies consistently identified a DR3-type VDRE as major VDR-binding sites, although within 100 bp of ChIP-Seq peak summits, only less than 40% of the peaks actually contain DR3.[15] Importantly, one of these studies showed that genetic loci associated with MS susceptibility detected by genome-wide association study (GWAS) are enriched for VDR-binding sites accumulated in active regulatory regions of chromatin.[12,22] The other study found the most significant relevance of upregulated VDR target genes to the intracellular signaling cascade by using the gene ontology (GO) analysis with GeneTrail.[13]

We found that the complex molecular network of 1541 calcitriol-responsive VDRTGs is functionally related to leukocyte transendothelial migration and Fcγ receptor-mediated phagocytosis. These observations propose a scenario that vitamin D deficiency in MS patients could cause aberrant regulation of leukocyte and macrophage functions by disorganizing autoregulatory loops of the molecular network. Migration of activated T cells and monocytes into the brain across the disrupted blood-brain barrier (BBB) plays a key role in the development of active demyelinating lesions in MS. Vitamin D reduces the clinical severity of experimental autoimmune encephalomyelitis (EAE), an animal model of MS, by stimulating T cell apoptosis and inhibiting monocyte recruitment in the CNS.[24] We identified CD99, a cell-surface glycoprotein involved in T cell migration and apoptosis,[25] as one of calcitriol-responsive VDRTGs, potentially serving as a novel therapeutic target for MS (Figure 3). TCR signaling upregulates VDR expression on T cells, and subsequently elevates the levels of expression of PLCG1, a signaling molecule pivotal for T cell activation.[26] We also identified PLGC1 as a calcitriol-responsive VDRTG (Supplementary Table 7 online).

NR4A2, a member of the nuclear receptor superfamily, whose expression is greatly upregulated in T cells of active MS patients,[27] plays a key role in differentiation of Th1, Th17, and Treg cells with relevance to induction of autoimmunity. We identified NR4A2 as a calcitriol-responsive VDRTG (Figure 4). Transcription factors RUNX1 and RUNX3 are essential for induction and suppressive function of Foxp3$^+$ inducible Treg (iTreg) cells,[28] and both are calcitriol-responsive VDRTGs (Supplementary Table 7 online), suggesting a crucial role of vitamin D in immune tolerance induction. Furthermore, we identified EBI3, a component of anti-inflammatory cytokine IL-35 produced mainly by Treg cells,[29] as a calcitriol-responsive VDRTG (Supplementary Table 7 online).

B cells play an active role in the immunopathogenesis of MS.[30] They constitute lymphoid follicle-like structures ectopically located in the meninges of secondary progressive MS (SPMS) patients. We identified CXCR5, the receptor for the B-cell attractant CXCL13 produced by monocytes,[31] as a calcitriol-responsive VDRTG (Supplementary Table 7 online). Importantly, vitamin D itself regulates development and functionality of B cells.[30] Fcγ receptors act as a major phagocytotic receptor of macrophages/monocytes and microglia for ingestion of opsonized myelin. The expression of FCER1G is elevated in chronic MS lesions, and FCER1G-knockout mice show improved recovery from EAE.[32] Fcγ receptor-mediated phagocytosis requires cell membrane extension with cytoskeletal organization regulated by Rho family GTPase proteins, such as Rac1 and CDC42.[33] We identified CDC42 as one of calcitriol-responsive VDRTGs (Supplementary Table 7 online).

In conclusion, we found that the molecular network of 1541 calcitriol-responsive VDRTGs is linked to leukocyte transendothelial migration, Fcγ receptor-mediated phagocytosis, and transcriptional regulation by VDR.

Downloaded from msj.sagepub.com at National Center of Neurology and Psychiatry on February 12, 2013